# Stability and Dewetting of Metal Nanoparticle Filled Thin Polymer Films: Control of Instability Length Scale and Dynamics

**Rabibrata Mukherjee,[†] Soma Das,[‡] Anindya Das,[‡] Satinder K. Sharma,[§] Arup K. Raychaudhuri,[‡] and Ashutosh Sharma[§,*]**

[†]Department of Chemical Engineering, Indian Institute of Technology Kharagpur, Pin 721 302, West Bengal, India, [‡]S. N. Bose National Centre for Basic Sciences, Block JD, Sector III, Saltlake, Kolkata 700097, India, and [§]Department of Chemical Engineering and DST Unit on Nanosciences, Indian Institute of Technology, Kanpur 208016, India

**ABSTRACT** We investigate the influence of gold nanoparticle addition on the stability, dewetting, and pattern formation in ultrathin polymer—nanoparticle (NP) composite films by examining the length and time scales of instability, morphology, and dynamics of dewetting. For these 10—50 nm thick ($h$) polystyrene (PS) thin films containing uncapped gold nanoparticles (diameter ~3—4 nm), transitions from complete dewetting to arrested dewetting to absolute stability were observed depending on the concentration of the particles. Experiments show the existence of three distinct stability regimes: regime 1, complete dewetting leading to droplet formation for nanoparticle concentration of 2% (w/w) or below; regime 2, partial dewetting leading to formation of arrested holes for NP concentrations in the range of 3—6%; and regime 3, complete inhibition of dewetting for NP concentrations of 7% and above. Major results are (a) length scale of instability, where $\lambda_H \sim h^n$ remains unchanged with NP concentration in regime 1 ($n \sim 2$) but increases in regime 2 with a change in the scaling relation ($n \sim 3$—3.5); (b) dynamics of instability and dewetting becomes progressively sluggish with an increase in the NP concentration; (c) there are distinct regimes of dewetting velocity at low NP concentrations; (d) force modulation AFM, as well as micro-Raman analysis, shows phase separation and aggregation of the gold nanoparticles within each dewetted polymer droplet leading to the formation of a metal core—polymer shell morphology. The polymer shell could be removed by washing in a selective solvent, thus exposing an array of bare gold nanoparticle aggregates.

**KEYWORDS:** thin film · dewetting · instability · patterns · nanocomposites

Thin polymer films find application in areas such as electronics, coatings of various types (optical, dielectric, thermal barrier, *etc.*), lubricants, adhesives, paints, biological membranes, *etc.*[1−4] However, in ultrathin films, typically thinner than ~100 nm, the issue of film stability becomes important as these films often become unstable and tend to rupture and dewet following a variety of mechanisms such as spinodal dewetting engendered by the van der Waal's interaction,[5−14] heterogeneous nucleation,[15−19] release of residual stresses accumulated during the film preparation,[20,21] density variations,[22,23] *etc.* Self-organization and pattern formation during dewetting of ultrathin polymer films result in the formation of an array of holes or droplets, as reported first by Reiter.[5,6] Controlled dewetting on topographically or chemically patterned substrates is suggested to be a viable route for the creation of ordered mesoscale surface patterns.[24−30] Dewetting induced structures have been utilized for the fabrication of organic field-effect transistors,[31] electronic devices,[32] biological applications such as cellular patterning,[33] *etc.* However, formation of defect-free, thin, stable and continuous coatings on a variety of substrates without substrate modifications is an extremely important aspect of coatings technology, which has not yet been fully addressed.

In most of the applications involving polymer thin films such as coatings, lubricants, paints, *etc.*, instability and dewetting are undesirable, and thus controlling the film integrity is a problem of both fundamental and technological importance. Several methods have been suggested to stabilize a thin film, examples of which include grafting of compatibility enhancing polymer layers at the film−substrate interface,[34] incorporation of specific end groups having affinity toward the substrate material,[35] metal complexation and sulfonation of a polymer,[36] phase segregation induced stabilization of polymer thin films (PS) by adding another polymer (PMMA) in low concentrations,[37] addition of miscible components such as tetramethylbisphenol in a PS film,[38] *in situ* photochemical cross-linking using photoactive filler bisbenzophenon molecules, *etc.*[39] A promising technique for achieving enhanced stability seems to be the addition of low quantities

*Address correspondence to ashutos@iitk.ac.in.

Received for review December 28, 2009 and accepted May 20, 2010.

**Published online June 18, 2010.**
10.1021/nn901912d

of nanoparticles or nanofillers to the polymer film, which can completely inhibit dewetting.[40−50] This was first reported by Barnes *et al.* with ultrathin polystyrene and polybutadiene thin films (20−50 nm) by the addition of low quantities (0.1−5% w/w) of fullerene nanoparticles.[40] The interactions between the polymer molecules and the nanoparticles lead to variations in properties such as the glass transition, viscosity, *etc.*, of the system.[51−63] Similar inhibition of dewetting due to the addition of various types of nanofillers such as polymer nanoparticles,[41] dendrimers,[42] *etc.*, was subsequently reported by other groups in a variety of settings. In most cases, it was suggested that the particles phase separate from the polymer and segregate to the film−substrate interface. This in turn alters the surface energy and consequently the wetting property of the substrate, resulting in a change in the nature of effective interaction between the film and the substrate. On the basis of molecular dynamics simulations, Luo *et al.* suggested that a combination of factors such as mobility of the nanofillers, their size, their interaction with the polymer chain, additional pinning effect imparted by the particles on the three-phase contact line, *etc.*, is responsible for the enhanced stability of the films.[43] In a similar study, Hosaka *et al.* reported the inhibition of dewetting of thin PS films containing polyhedral oligomeric silsesquioxane (POSS) and cyclopentyl-substituted POSS (CpPOSS) nanoparticles (diameter ∼1−3 nm), due to segregation and subsequent crystallization of the silsesquioxane molecules on the substrate.[44] The same strategy of nanoparticle addition has also been successfully utilized for inhibiting instability in thin polymer bilayers[46−48] and block copolymer thin films.[49] However, it is shown that for bilayer systems, dewetting can also be accelerated, depending on the nature of particle−polymer interaction.[46−48] Thus, the issue of kinematic stability, in addition to thermodynamics of the system, also becomes an important factor in the stabilization of nanoparticle-filled polymer films.[48] For bilayer systems, Xavier *et al.* have shown that even when polymer−matrix interactions are unfavorable, dewetting can be kinematically inhibited by controlling the relative size of the particles and the length of the polymer chain, which in turn affects the rheology of the system.[47] In a similar fashion, Koo *et al.* with multiwalled carbon nanotube fillers have shown the influence of aspect ratio of the tubes on the rheology and stability of the films.[48] Their work suggests that longer nanotubes were more effective in inhibiting dewetting by forming entangled networks that prevented long-range motion of the polymer. In a recent work, Hosaka *et al.* have shown that, in thin PS films, the inhibition of dewetting is a function of the filler concentration.[50] While for high concentration of CpPOSS, dewetting was completely inhibited, for lower concentration of the filler, there was partial dewetting of the films. The dewetting in films with lower particle concentration is explained in terms of partial coverage of the film substrate by the segregated particles.[50]

In this paper, we examine the solvent vapor induced dewetting of thin polystyrene (PS) films (thickness: 12−42 nm) containing *uncapped* gold nanoparticles on silicon wafers with ∼1.5 nm native oxide layer. In order to critically examine the mechanisms of dewetting in nanocomposite thin films, we characterize the influence of NP concentration on the early stages of the growth of instability by quantifying its length scale and dynamics before formation of holes. Dynamics, morphology, and NP distribution and aggregation are also studied in the later stages of the hole growth, coalescence, and droplet formation. We thus find and characterize three distinct regimes of dewetting and instability. Regime 1: Complete dewetting for low particle concentration (less than 2%, wt of particle/wt of polymer), leading to the formation of an isotropic array of polymer droplets. Regime 2: Partial dewetting for intermediate particle concentration (3.2−6.4%) up to the stage of hole formation, including initiation of hole coalescence (in some cases). Regime 3: Complete inhibition of dewetting for films with particle concentration above 7%. The second major objective is to relate the length scale of the instability to the particle concentration and film thickness for completely and partly dewetting films (regime 1 and regime 2). It is well-known that, for spinodal dewetting of homopolymer thin films without any filler particles, the length scale of the structures (holes) ($\lambda_H$) corresponds to the fastest growing mode of instability and is a strong function of the film thickness ($\lambda_H \sim h^n$; $n \sim 2$).[5−15] Our observations suggest that, for regime 1 films, there is no quantitative or qualitative change in the length scale of the structures as a function of nanoparticle concentration ($n \sim 2$). For the regime 2 films, there is a gradual increase in the length scale of instability ($\lambda_H$) as well as a significant change in its scaling relation with increase in the particle concentration. Finally, the films become completely stable in regime 3 ($\lambda_H \rightarrow$ infinity). Our observations reveal that the transition from complete dewetting to complete stability is associated with a gradual increase of the instability length scale. Third, we report in detail two critical matters related to regime 1 films: (1) the influence of NP concentration on dewetting dynamics, and (2) the structure of individual dewetted droplets, particularly the conformation of the gold particles within each dewetted droplet. On the basis of *in situ* experiments, we show that, for a particular film thickness, the dewetting dynamics becomes progressively sluggish with enhanced particle concentration. In addition, we have also found that, for very low particle concentration (as well as for particle-free films), dewetting is accomplished in two clear and distinct stages: a rapid initial phase followed by a slower late stage. However, as the particle concentration increases, the distinction between these two stages becomes diffused, and for films

with 2.0% nanoparticle concentration, a uniform dewetting velocity is observed. Lastly, detailed investigation of individual dewetted droplets by force modulation AFM and micro-Raman experiments revealed that there is a phase segregation and accumulation of the nanoparticles toward the center of each droplet. Each dewetted droplet thus has a core−shell morphology; the core comprising a self-assembled aggregate of the nanoparticles, and the surrounding shell is constituted by the dewetted polymer. Finally, we show that the polymer shell can be selectively removed, which results in an array of isolated aggregates of gold nanoparticles.

The observations related to length scale, dynamics, and morphology are critically examined in view of the existing theories on the roles of NP aggregation, slippage, viscoelasticity, and heterogeneities on thin film rupture.

## RESULTS AND DISCUSSION

**Effect of Nanoparticle Concentration on Film Stability.** As mentioned briefly in the previous section, depending on the nanoparticle concentration, we found that there are three distinct regimes of dewetting: complete dewetting leading to hole coalescence and droplet formation, partial dewetting characterized by arrested hole growth, and complete inhibition of hole formation. For 12−42 nm thick polystyrene (PS) films exposed to toluene (solvent) vapor, the limits of particle concentrations for each clearly distinguishable regime were found to be as follows: regime 1, particle concentration = 0−2.0%; regime 2, NP concentration = 3.2−6.4%; regime 3, NP concentration = 7.0% and above.

The final morphology of a thin film of constant thickness but with different particle concentrations falling in different regimes is shown in Figure 1. Figure 1A shows the fully dewetted morphology of a 17 nm thick film, having NP concentration of 1.0%, exposed to solvent vapor for ~3 h. Further exposure to solvent vapor for prolonged time (~18 h) did not alter the morphology of the structures to any major extent. For comparison, the morphology of a fully dewetted film (exposed to vapor for 15 min) of the same thickness but without any nanoparticles is shown in Figure 1B. By mere visual observation, it can be seen that the two micrographs are nearly identical. The intermediate morphologies of both films were also quite similar during the dewetting process, though the time scales were different (discussed in detail later). The partially dewetted final morphology of the regime 2 films of same thickness (17 nm) is shown in Figure 1C,D. Dewetting progressed until coalescence of hole rims for films with NP concentration of 3.2% (Figure 1C). However, for films with 6.4% NP concentration, dewetting propagated only to the extent of formation of a few isolated holes, as can be seen in Figure 1D. An interesting observation involving

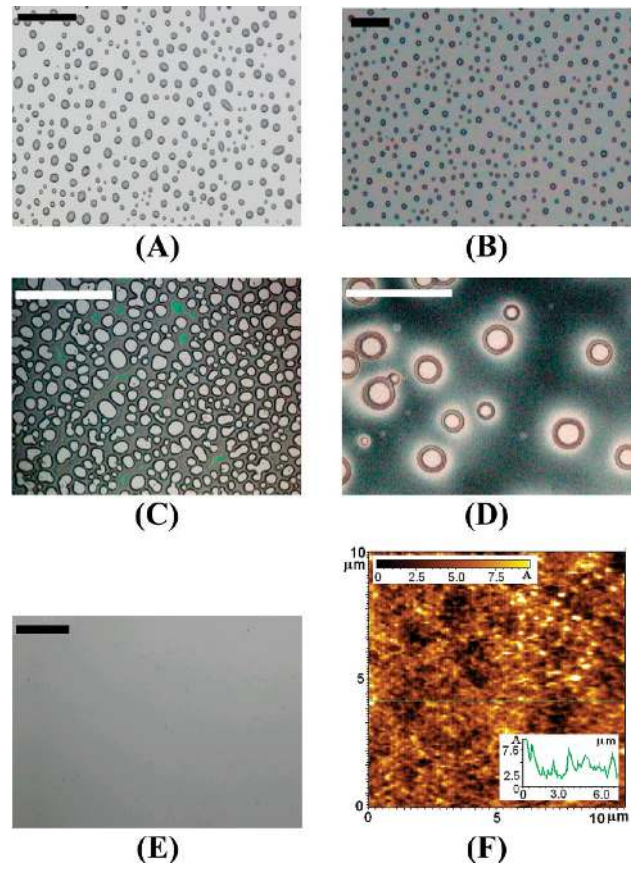


**Figure 1. Influence of NP concentration on the final morphology of the PS films exposed to toluene vapor. Completely dewetted structure for regime 1 films: (A) 1.0% NP concentration, exposure time = 3 h; (B) no particle, exposed for 12 min. Partial dewetting for regime 2 films, after 60 h of exposure: dewetting up to the level of (C) coalescence of rims for a film with NP concentration of 3.2% and (D) up to formation of holes for a film with 6.4% NP concentration. (E) Completely stable film after 60 h of solvent vapor exposure when the NP concentration was 8.0% (regime 3). (F) AFM image of a stable (regime 3) film, showing a smooth film surface (rms roughness <1 nm) with no surface undulations after 60 h of solvent vapor exposure. Film thickness = 17 nm and scale bar = 30 μm in all micrographs (A−E).**

Figure 1C,D is that although the film thicknesses are same in both cases, the holes appear to be slightly larger in Figure 1D compared to Figure 1C. We attribute this to the coalescence of holes in the case of Figure 1C (and also in most other dewetting experiments) before the holes grow to their maximum possible size, which happens in the case of Figure 1D, as there appears to be less number of holes at higher nanoparticle concentration. The micrograph in Figure 1E shows the surface of a completely stable film with 8.0% NP (regime 3). In all these cases (Figure 1C−Figure 1F), the films were exposed to solvent vapor for 60 h to ensure that there was no subsequent evolution of the surfaces. In order to ascertain if the topography of the stable regime 3 films was truly flat or carried some signature of any instability in the form of surface undulations, the films were further investigated using AFM (Figure 1F). The cross-sectional line scan shown in the inset of Figure 1F confirms that the RMS roughness was less than

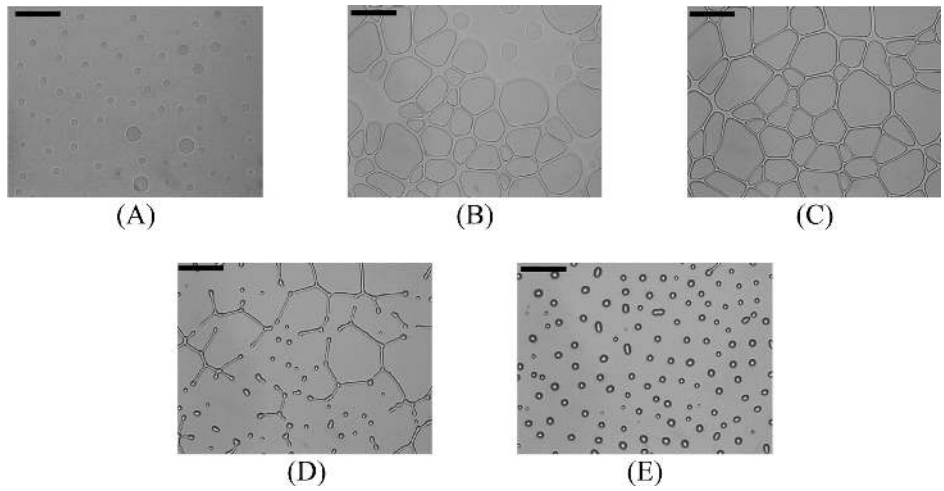


**Figure 2. Morphological evolution at different stages of solvent (toluene) vapor induced dewetting of a 23 nm thick PS film with 1.0% nanoparticle concentration, on a cleaned silicon wafer substrate. (A) After exposure to toluene vapor, 40 min initiation of dewetting with the formation of random holes; (B) 90 min solvent vapor exposure leads to formation of more holes and their growth. (C) After 140 min solvent vapor exposure, the growing holes coalesce to form interconnected ribbons of polymers. (D) Partially broken rims due to Rayleigh instability after 165 min and (E) completely dewetted morphology comprising an isotropic array of droplets after 5 h of solvent vapor exposure. Scale bar in all cases = 20 μm.**

~1 nm, and therefore, it is reasonable to conclude that a regime 3 film remains smooth without any signature of instability even after prolonged solvent vapor exposure, clearly distinguishing themselves from regime 1 and regime 2 films. The subsequent sections deal with the largely unexplored dynamics and morphological evolution of regime 1 films. It may be noted that extensive studies are already available[40−50] on the dynamics of evolution of partially stable regime 2 nanocomposite thin films.

**Dewetting and Morphological Evolution of a Regime 1 Nanocomposite Film.** This section describes the morphological evolution sequence of a dewetting film that has particle concentrations corresponding to regime 1. A representative example is shown in Figure 2 for the solvent vapor induced dewetting of a 23 nm thick PS film with NP concentration of 1.0%. The onset of instability was observed after solvent vapor exposure of ~32 min, with the formation of a few isolated but nearly equally sized holes (Figure 2A). Further progress in dewetting led to the growth of the holes as well as the appearance of some new holes. Morphology of the film corresponding to this stage is shown in Figure 2B, which was attained after ~90 min of solvent vapor exposure. With further solvent vapor exposure for ~140 min, the rims of the adjacent growing holes started to touch each other, as shown in Figure 2C, forming a cellular network comprising polymer ribbons. Immediately beyond this stage, the ribbons started breaking down into fragments due to the Rayleigh instability, as shown in Figure 2D. In the final stages of dewetting (~5 h of solvent vapor exposure), the elongated polymer fragments retracted further and formed well-rounded polymer droplets (Figure 2E). Beyond this stage, the morphology remained unaltered even after solvent vapor exposure for several hours (~60 h), indicating the formation of the final equilibrium structures. The image sequence in Figure 2 clearly indicates that morphological evolution for a regime 1 film closely resembles the *classic* dewetting scenario of a polymer thin film on a silicon wafer or quartz substrate.[5−13]

**Influences of Nanoparticle Concentration on the Length Scale of Instability for Regime 1 and Regime 2 Films.** Spontaneous instability and dewetting of an ultrathin liquid polymer film is engendered by the amplification of capillary waves at the film surface. In the absence of an externally imposed field such as an electric field[63] or a thermal gradient,[64] attractive van der Waal's interaction between the film−air and film−substrate interface acts as the main destabilizing influence, resulting in spontaneous rupture and dewetting of the film. On the basis of theoretical analysis and simulations, it has been shown that the action of the two antagonistic forces (the destabilizing van der Waal's interaction and the stabilizing surface tension forces) may result in the amplification of a narrow band of capillary waves,[5−16] eventually resulting in the rupture and hole formation in the film. The holes, though randomly located, are found to be isotropically distributed in dewetting experiments, and there is typically a mean distance between the holes corresponding to the wavelength of the amplified capillary waves or the dominant length scale of instability ($\lambda_H$), which shows a scaling with the film thickness ($h$) as $\lambda_H \sim h^2$, in cases where the dewetting is engendered by the nonretarded van der Waal's interaction. Similarly, the scaling relation between the maximum number density of the holes ($N_H$) and $h$ is given as $N_H \sim h^{-4}$; $\lambda_H$ and $N_H$ has been independently measured for each dewetting experiment based on FFT of micrographs corresponding to the stage where the number density of holes passes through a maxima. It may be pointed out that, in typical dewetting experi-

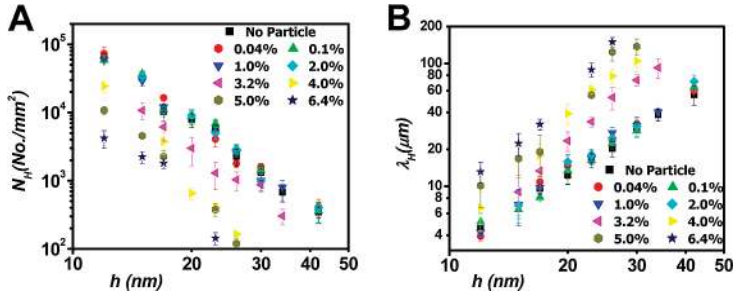


**Figure 3. Log−log plots of (A) maximum number density of holes ($N_H$) and (B) periodicity or length scale of the holes ($\lambda_H$) as a function of initial PS film thickness ($h$) for different nanoparticle concentrations for regime 1 and regime 2 films. The best fit to the data (lines not shown on the plot) are presented in Table 1.**

ments, the number density of holes ($N_H$) gradually increases with time as more and more holes appear in the initial stage of dewetting. It remains nearly constant when the holes grow in the intermediate stages, without the appearance of any additional holes. With further progress in time, the number density of holes starts to gradually reduce due to coalescence of adjacent holes. Thus, $N_H$ and $\lambda_H$ pass through a maximum and a minimum, respectively, in any dewetting experiment, and the values of $N_H$ and $\lambda_H$ corresponding to this stage are subsequently used in analyzing the length scales of dewetted structures. The length scale exponents are obtained from the best fit obtained from the plots of $\lambda_H$ *versus* $h$ and $N_H$ *versus* $h$ on double logarithmic axes, respectively. As briefly mentioned before, if these values of the exponents are experimentally found close to 2 or −4 (respectively), it is argued that the film has ruptured due to the interaction of the nonretarded van der Waal's forces.[5−11] However, an equally strong alternative explanation of dewetting, especially for high molecular weight polymer films, is proposed based on the release of residual stresses accumulated during the film preparation.[20,21] Regardless of the precise mechanism of dewetting, the exponent for the dependence of the length scale on the film thickness seems to be within a narrow range.[10]

The results of dependence of $N_H$ and $\lambda_H$ with $h$ for different NP concentrations for regime 1 and regime 2 films are shown in Figure 3A,B, respectively. The corresponding values of $N_H$ and $\lambda_H$ for particle-free films in the same thickness range are also plotted on the same graphs in order to directly contrast the results as to how the $N_H$ and $\lambda_H$ vary for NP-filled and particle-free films. The film thicknesses used for the experiments were in the range of 12−42 nm, and particle concentration was varied between 0.1 and 6.4%, covering both regime 1 and regime 2 films. For every NP concentration−thickness combination, at least four samples were prepared in separate batches in order to test the repeatability of the experiments and to generate a highly robust data set. The best linear fit to the data on a double logarithmic plot for each NP concentration is presented in Table 1. It can be clearly seen in Figure 3A,B, as well as from the values of the exponents to the best fit in Table 1, that for regime 1 films (NP concentration <2.0%), the data points corresponding to a specific film thickness nearly coincide with each other, irrespective of the NP concentration. Also, relatively lower values of the error bars (within ∼5%) on the exponents of the best fit for Regime 1 films in Table 1 suggest that the points ($N_H$ *vs* $h$ and $\lambda_H$ *vs* $h$, respectively, for each NP concentration) are well represented by the best fit on the log−log plot (best fits not shown on plot). Thus, it is obvious that, for low NP concentrations (regime 1), there is no major change in the nature of the destabilizing forces responsible for dewetting, as compared to a particle free film, irrespective of the precise mechanism of dewetting. Regardless of the exact mechanism, an "effective" Hamakar constant ($A_E$) representing the strength of the destabilizing force has been calculated for comparison. The periodicity of the holes ($\lambda_H$) obtained from the FFT of the images has

**TABLE 1. Relation between the Periodicity of the Holes ($\lambda_H$) and the Maximum Number Density of the Holes ($N_H$) with Film Thickness ($h$)**

| particle concentration | extent of dewetting | $\lambda_H$ *vs* $h$ scaling | $N_H$ *vs* $h$ scaling | $A_E$ (effective Hamaker constant, J) |
|---|---|---|---|---|
| no particle | complete | $\lambda \sim h^{2.0177\pm0.0951}$ | $N_H \sim h^{-4.104\pm0.146}$ | $(2.632 \pm 0.117) \times 10^{-20}$ |
| 0.04% | complete | $\lambda \sim h^{2.1829\pm0.1056}$ | $N_H \sim h^{-4.295\pm0.230}$ | $(2.874 \pm 0.135) \times 10^{-20}$ |
| 0.10% | complete | $\lambda \sim h^{2.2186\pm0.1536}$ | $N_H \sim h^{-3.912\pm0.108}$ | $(2.239 \pm 0.094) \times 10^{-20}$ |
| 1.0% | complete | $\lambda \sim h^{2.1398\pm0.1251}$ | $N_H \sim h^{-4.231\pm0.109}$ | $(2.123 \pm 0.122) \times 10^{-20}$ |
| 2.0% | complete | $\lambda \sim h^{1.9778\pm0.2315}$ | $N_H \sim h^{-4.083\pm0.256}$ | $(2.007 \pm 0.312) \times 10^{-20}$ |
| 3.2% | partial | $\lambda \sim h^{3.2825\pm0.4655}$ | $N_H \sim h^{-4.883\pm0.456}$ | |
| 4.0% | partial | $\lambda \sim h^{3.0348\pm0.3964}$ | $N_H \sim h^{-6.393\pm0.359}$ | |
| 5.0% | partial | $\lambda \sim h^{3.055\pm0.3823}$ | $N_H \sim h^{-6.152\pm0.729}$ | |
| 6.4% | partial | $\lambda \sim h^{3.3444\pm0.593}$ | $N_H \sim h^{-5.806\pm0.840}$ | |

been used for the calculations. The dominant length scale of the features (holes), $\lambda_H$, is related to the magnitude of the destabilizing force, $-\Delta G''$,[13,65] as

$$\lambda_H = [(8\pi^2\gamma)/(-\Delta G'')]^{0.5} \quad (1)$$

where $\Delta G''$ is the second derivative of the excess free energy of interaction per unit area ($\Delta G$) with respect to the thickness of the film (h). Substituting the expression for $\Delta G''$ for the van der Waals interaction, $\Delta G'' = [A_E/(2\pi h^4)]$ into eq 1 and its subsequent rearrangement, the expression for the effective Hamaker constant ($A_E$), which has been used to calculate the values of $A_E$ listed in Table 1, is obtained as

$$A_E = [(16\pi^3\gamma h_B^4)/\lambda_H^2] \quad (2)$$

In our calculations, the surface tension of PS has been taken as 31.2 mJ/m$^2$.[2,29,30] It is worth pointing out that the value of $A_E$ for particle-free films obtained from our experiments ($\sim 2.6 \times 10^{-20}$ J) is close to previously reported values of $A_E$ for dewetting of PS films on a silicon wafer substrate with native oxide layer, which are in the range of ($\sim 1.8-2.2$) $\times 10^{-20}$ J.[13,65] Further, it is seen in Table 1 that $A_E$ values remain nearly independent of NP concentration for regime 1 films and are also close to that for particle-free films. A slight reduction in $A_E$ with an increase in NP concentration can be seen upon careful observation of Table 1. However, we feel that this change is not significant as it is within the error bars.

In contrast, for regime 2 films, the length scale of instability is found to depend strongly on NP concentration, and the corresponding values of $N_H$ and $\lambda_H$ deviated significantly from those of particle-free and regime 1 films having the same thickness. This is clearly seen in Figure 3A,B. Fewer holes appear over the same area for a partly dewetting regime 2 film, as compared to a particle-free or regime 1 film having the same thickness. This results in a higher value of $\lambda_H$ between the structures. Also, unlike regime 1 films, where $N_H$ and $\lambda_H$ values depend only on *h* and remained largely independent of the exact NP concentration, in regime 2 films, the values of $N_H$ and $\lambda_H$ are found to be strong function of the NP concentration even for films with the same thickness. In regime 2 films, the maximum number density of holes gradually ($N_H$) decreases, and concurrently, the structure periodicity ($\lambda_H$) increases with increase in NP concentration for films having the same thickness.

Also it is evident that there exists a critical NP concentration at which transition from regime 1 (complete dewetting) to regime 2 (partial dewetting) occurs. For our system, this cutoff lies between 2.0 and 3.2% NP concentration but cannot be determined with a greater precision. A possible reason for partial dewetting in regime 2 films is discussed later, based on micro-Raman analysis.

**Influence of Nanoparticle Concentration on Dewetting Dynamics and Extent of Dewetting.** While there was no tangible influence of NP concentration on the instability length scale for regime 1 films, the dewetting dynamics showed strong dependence on NP concentration, as it became progressively sluggish with increase in the gold nanoparticle concentration. This particular aspect was investigated in detail by studying *in situ* dewetting of 23 nm thick PS films with the following nanoparticle concentrations: 0.04, 1. 0, and 2.0% (shown in Figure 4B−D, respectively). *In situ* experiments with particle-

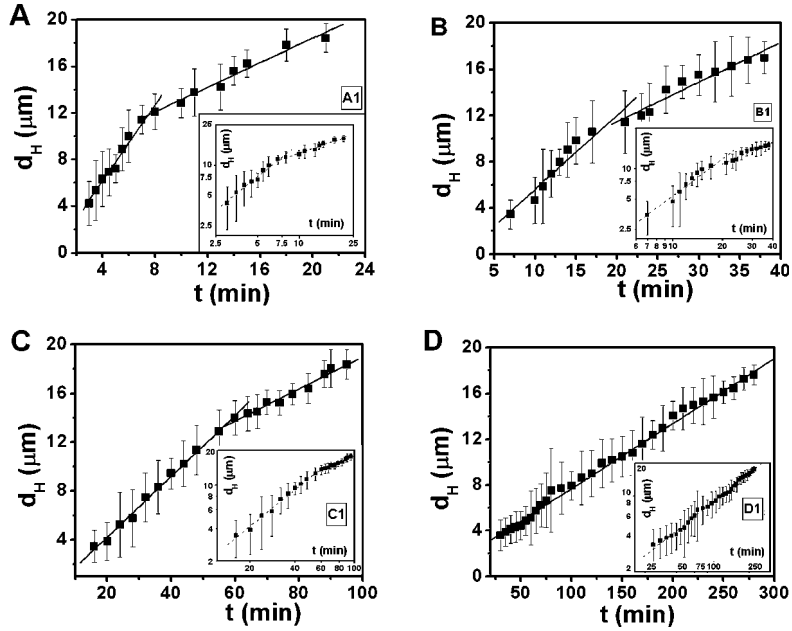


**Figure 4. Plots of average hole diameter *vs* dewetting time for 23 nm thick regime 1 film with (A) no particles, (B) particle concentration = 0.04%, (C) particle concentration = 0.10%, (D) particle concentration = 2.0%. Insets show the same data on a log−log scale. Straight lines show the best fit to the data.**

**TABLE 2. Calculated Dewetting Velocity for 23 nm Thick Nanocomposite Films with Different NP Concentrations**

| particle concentration | dewetting velocity stage I ($V_{D1}$, μm/min) | dewetting velocity stage II ($V_{D2}$, μm/min) | ratio ($V_{D2}/V_{D1}$) | time scale exponent ($n_1$) stage I | time scale exponent ($n_2$) stage II |
|---|---|---|---|---|---|
| no particle | 1.6370 ± 0.09418 | 0.61177 ± 0.04411 | 0.371 | 1.1621 ± 0.0517 | 0.6221 ± 0.06162 |
| 0.04% | 0.6304 ± 0.06287 | 0.34328 ± 0.03264 | 0.544 | 1.2082 ± 0.1051 | 0.7091 ± 0.08156 |
| 0.10% | 0.2494 ± 0.00568 | 0.17147 ± 0.00745 | 0.687 | 1.1197 ± 0.0348 | 0.6199 ± 0.03898 |
| 2.0% | $V_D$ = 0.05681 ± 0.00289 | | | $n$ = 0.72331 ± 0.06049 | |

free PS thin films having the same thickness were also performed (Figure 4A) in order to contrast the dynamics of nanocomposite films with particle-free films. For each NP concentration, *in situ* dewetting experiments with at least four samples were performed, and in every sample, the temporal growth of five holes were tracked. Thus, every point on any plot in Figure 4 corresponds to averaging over many numbers of experimental observations, which in turn is responsible for relatively large error bars in some cases. Slopes of the best fit to the data in plots in Figure 4A−D have been utilized to find the average dewetting velocity ($V_D$, calculated as the average growth rate of diameter in μm/min). In addition, the exponent of the average hole diameter with time of dewetting ($D_H \sim t^n$) was found from the best fit of the same data on double logarithmic plots (shown in the insets of the respective plots). The average dewetting velocity as well as the time scale exponents for the films investigated is presented in Table 2.

Two major observations emerge from the plots shown in Figure 4: (a) the dynamics of dewetting becomes progressively slower as the NP concentration increases, and (b) the dewetting velocity shows a two-stage trend for the particle-free films as well as for films with low NP concentrations (up to 1.0% in our experiments, Figure 4A−C). However, for 2.0% NP concentration, this trend disappears and dewetting progresses at a nearly constant velocity all through.

The slower dynamics of the nanocomposite films with enhanced NP concentration is manifested in two ways: (a) in terms of longer solvent vapor exposure time for the appearance of the first hole as well as time taken to reach the stage where the holes start coalescing, and (b) in terms of slower dewetting velocity. While longer time scales of dewetting are qualitatively manifested in the plots in Figure 4, some quantitative data in that regard are reported here. While the onset of film rupture with the appearance of the first set of holes was seen after ∼3.5 ± 1 min for particle-free films of 23 nm thickness, the time requirements for the same stage were ∼7.0 ± 1.5, ∼18.0 ± 2, and ∼34.0 ± 4 min, respectively, for films with 0.04, 1.0, and 2.0% NP concentrations under identical experimental conditions. Similarly, the time at which the holes start to merge was also prolonged as the NP concentration increased. While it took ∼21 ± 2 min for the rims of the adjacent holes to start coalescing for a particle-free film, ∼ 38 ± 3, 95 ± 6, and 275 ± 12 min were needed for films with 0.04, 1.0, and 2.0% NP concentrations, respectively, to reach the same stage. Obviously, the time taken for complete dewetting also showed a similar trend, extending from ∼40 min for particle-free films to ∼2.0, ∼ 3.5, and ∼10.5 h for films with 0.04, 1.0, and 2.0% NP concentrations, respectively. Interestingly, the average diameters of the holes corresponding to the time when the rims of the adjacent holes started to merge with each other were found to be nearly same in all cases (∼17 ± 1.2 μm). This value was found to be independent of the nanoparticle concentration and was nearly the same (within error bars) for the particle-free films also. This observation is in line with our earlier claim that there is no tangible influence of NP concentration for the regime 1 films on the length scale or size of the dewetted features. Table 2 lists the dewetting velocities and the time scale exponents ($n$) based on the plots in Figure 4.

We now critically examine the possible mechanisms responsible for the change in instability length and time scales and their observed dependence on particle concentration. The addition of nanoparticles could conceivably modulate (A) slippage of the film on its substrate[12,69,70] or (B) rheology (viscoelasticity) of the film[12,66−68,72] or (C) introduce an additional heterogeneous nucleation-based mechanism for rupture.[12,17,24−26] We examine the consequences of each of these factors vis-à-vis our experimental observations on the length and time scales of dewetting.

With regard to slippage, it may be induced possibly by either particle segregation at the film−substrate interface or a weak network formation because of anchoring of polymer chains on nanoparticles.[52−62] It is known[12,69,70] that, in the so-called weak slip regime (slip length ∼ film thickness), the length scale of the instability and its thickness dependence are largely unaffected, as is also observed in our experiments. However, any amount of slip greatly accelerates the dynamics of instability and hole growth, whereas just the reverse is observed here. Further, the length scale exponent is substantially smaller in the strong slip regime compared to 2, whereas the experiments show an *increase* of this exponent (Table 1). Thus, slippage may be ruled out as a causative factor in explanation of our results.

With regard to rheology, it is known that particle−polymer nanocomposites can exhibit signifi-

cant changes in glass transition temperatures as well as enhancements in viscoelastic properties.[51−62] The changes in properties are typically attributed to the high surface area to volume ratios of the filler particles.[52] The individual polymer molecules of a homopolymer can also be anchored and thus be cross-linked around the particles, leading to higher viscosity and even viscoelasticity.[52−62] It is known that viscosity, being a transport property, does not affect the length scale of instability but merely slows down its dynamics.[66−68,72] This is in accord with the observations for regime 1 (low NP concentrations) but does not explain the results of regimes 2 and 3 films, where the length scale and its scaling with the film thickness change very substantially. Could introduction of viscoelasticity explain it? At least at low NP concentrations, the viscoelasticity is expected to be liquid-like without a significant permanent (zero-frequency) solid-like elastic modulus. For viscoelastic melts, it is known[68,72] that introduction of elasticity also does not change the instability wavelength but makes the growth of instability and the hole much faster! Observations show just the opposite across all the regimes. Further, a change in the length scale in regime 2 is also not in agreement with this scenario. At high NP concentrations, one could possibly argue for the existence of a solid-like viscoelasticity engendered by a strong interaction between the particles resulting in filler networks that span sections of the polymer matrix.[59] Such transitions from liquid-like viscoelasticity to solid-like viscoelasticity have been previously observed.[60−62] Recent theoretical studies[66,67,71] show that an ultrathin viscoelastic solid film, *when unstable*, indeed has the same fastest growing length scale of the instability as a viscous film *and* at the same time, the growth of instability is retarded because some of the destabilizing energy gets stored in the form of elastic deformation of the film. These theoretical results *seem* to be in accord with the observations, at least in regime 1, where the length scale remains unaffected. However, a closer examination excludes this mechanism because the van der Waals force or any other force of the magnitude implied in Table 1 is not strong enough to trigger the instability even in a very soft solid (elastic modulus $<$10 Pa!) film if it is thicker than about 10 nm.[66,67,71] Further, the change in the length scale in regime 2 is also not commensurate with this mechanism. The only speculative possibility that remains is that the solid-like viscoelasticity may play a role in the later stages of hole arrest in regime 2 and stable films of regime 3, where NP concentration is high (regime 3) or may become locally high in some part of the hole rim during later stages of dewetting (regime 2). We find some indication of the latter, which is discussed in the next section. High NP concentration together with a longer time available for aggregation and/or network formation in the slow regimes 2 and 3 could underlie the hole arrest.

Finally, with regard to a heterogeneous nucleation-based mechanism,[17,24−26] introduction of physicochemical nucleation sites by possible aggregation of particles should produce a different length scale for the instability and rupture, governed in part or wholly by the density of sites, rather than the well-defined spinodal scales witnessed in regimes 1 and 2. Further, the growth of instability by this energetically favorable pathway should be faster rather than slower!

The main purpose of the above discussion is to critically examine the possible pathways of instability in the NP-filled films in view of the length and time scales reported here for the first time. Perhaps there is no single mechanism but a combination of several factors, and their interplays that produce the observed length and time scale behavior. It may also be pointed that, in the system studied here, there was no aggregation of NPs observed at the interfaces either at the stage of film preparation (refer to online Supporting Information) or immediately after the hole formation, but only at later stages of hole growth and droplet formation. In other systems, where aggregation is prominently observed, the precise mechanism by which it may modulate the length and time scales in different regimes is not clear. The above discussion thus serves to stimulate further work in the area with special attention to the possibility of discriminating the exact mechanism based on the instability length and time scale considerations.

**Dewetting Velocity of Regime 1 Films.** It has been briefly mentioned that, for particle-free and low NP containing films (up to 1.0%), there is a distinct two-stage trend in the dewetting velocity (Figure 4A−C). In all these cases, the radius of the holes grow rather rapidly in the first stage, until the average diameter of the holes became $\sim 12 \pm 2$ μm. After this stage, a distinct transition in the growth rate of the holes is observed and the dewetting velocity drops considerably. As can be seen in Table 2, this relative difference in dewetting velocities of the two stages gradually reduces as the NP concentrations in the films progressively increase ($V_{D2}$ varying from ~37% of $V_{D1}$ for particle-free films to about ~68% of $V_{D1}$ for films with 1.0% NP concentration). This relative difference disappears with further increase in the NP concentration. For films with 2.0% NP concentration, only a monotonic trend in dewetting velocity is observed. Some experiments with intermediate NP concentrations (between 1.0 and 2.0%, results not shown in detail) showed that around a critical NP concentration of ~1.7% the transition from two-stage dewetting to a single-stage dewetting occurs. As can be seen in Table 2, dewetting velocity in nanocomposite films is up to 2 orders lower as compared to particle free films, indicating significantly slower dynamics that might allow reorganization of particles such as aggregation, segregation, and network formations.

There have been observations and theories of two or three distinct stages in dewetting of thin polymer

films.[73−76] Different relative magnitudes of the uncompensated Young's force causing dewetting, and the mechanisms of friction/dissipation lead to different regimes of dewetting. Theoretically, the three stages suggested by Brochard *et al.*[73] are as follows. Stage 1: In this stage, the instability is rapid compared to the translational (reptation) relaxation time of the polymer chains, resulting in a rapid early growth of the holes. The radius of the hole shows an exponential dependence on time ($D_H \sim \exp(t/\tau)$). In the subsequent stages, the time scales are sufficiently long[73] for the translational motion of the chains causing flow. In this stage, it is assumed that the viscous force balances the capillary driving force, and there is no slippage at the film−substrate interface. For these conditions, it has been theoretically predicted, as well as experimentally observed, that $R$ shows a linear dependence with time ($D_H \sim t$). In the third stage of dewetting, it is argued that there is a greater influence of slippage. The frictional resistance in slippage, which depends on the width of the rims, results in the decreased rate of hole growth. Theoretically, $D_H$ shows a time exponent of 2/3 in this regime ($D_H \sim t^{2/3}$).

For particle-free films and the regime 1 films showing two-stage dewetting (0.04 and 1.0% NP concentrations), the time scale exponents for the first stage ($n_1$) of dewetting are close to ~1 for all three cases (Table 2). From the preceding discussions, it is clear that this regime corresponds to the stage 2 discussed earlier, with very little influence of slippage. The second stage exponents ($n_2$) for all three cases are again close to (within error bars) the theoretically predicted value of 2/3, which signifies a strong influence of slippage in this stage of dewetting. A uniform value of $n \sim 0.72$ (again close to 2/3) for nanocomposite films with 2.0% NP concentration suggests that as the NP concentration goes up in regime 1 films, stronger influence of slippage becomes evident right from the early stages of dewetting. However, Al Akhrass *et al.* in a recent paper attributed longer relaxation time in viscoelastic polymer films to be responsible for two-stage dewetting.[76] Further investigations are underway to understand the exact mechanism and the particle−polymer interactions that influence the slippage at the interface.

It may, however, be noted that dewetting velocity ($V_D$) in general exhibits a nonlinear dependence on time (as seen in Table 2), irrespective of the particle concentration. $V_D$ is thus never really constant. For low NP concentration films (<1.0%), the first stage exponent $n_1$ is close to 1, indicating nearly a constant dewetting velocity ($V_{D1}$) for this stage. However, representing an average velocity $V_{D2}$ in the later stage is only for an easy comparison demonstrating the drop in the order of dewetting velocity as compared to the initial stage.

We have thus far discussed how the NP concentration influences the dewetting length scales and dynamics in regimes 1 and 2 films. We now focus on understanding of the possible mechanisms for the inhibition of dewetting at an intermediate stage in regime 2 films. Subsequently, we also look at another relevant issue associated with the dewetting of regime 1 films: how do particles distribute within each dewetted droplet? Do particles remain evenly distributed within the dewetted droplets or do they phase segregate? If they phase segregate, do they come to the substrate−polymer interface or the polymer−air interface? These investigations are extensively based on micro-Raman analysis using 500 nm $Ar^+$ laser spot size. The details about the technique are available in the Methods part.

**Inhibition of Dewetting at Intermediate Stage for Regime 2 Films.** In order to understand whether there is a phase segregation or deposition of particles from the retracting contact line of a growing hole in a regime 2 film, micro-Raman analysis was performed on the rim of a hole of a 17 nm thick film with 6.4% NP concentration (Figure 5A). This particular film dewetted only to the extent shown in Figure 5A, and subsequently the diameter of the hole remained unaltered even after prolonged solvent vapor exposure. Micro-Raman spectra at different locations in the vicinity of the rim (as marked in Figure 5A) are shown in Figure 5B−F. The spectrum at location 1 (Figure 5B) is from the dewetted portion of the sample. The spectrum shows only a peak corresponding to silicon and virtually no existence of either gold or polymer, suggesting no phase segregation or deposition of gold particles on the substrate surface during the retraction of the contact line. Location 2 corresponds to that part of the rim which is right adjacent to the hole. Location 3 corresponds to the point where (roughly) the rim height passes through a maxima, and location 4 is over an area where the height of the rim gradually starts reducing. Location 5 corresponds to an area where the rim merges with the film. It is interesting to note that there is virtually no signature of gold in the spectrum at location 2 (Figure 5C). In contrast, there are strong gold peaks at both locations 3 and 4 (Figure 5D,E, respectively), indicating lateral redistribution of gold particles within the rim. It appears that the central part of the hole rim has an enhanced concentration of particles, and depletion zones surround it near the contact line and near the far end of the rim. This is shown schematically in Figure 5G. Thus, in regime 2, a high local NP concentration exceeding a critical value, or a large available time allowed by a slow dynamics, may lead to particle aggregation. Similar aggregation of particles in droplets at late stages of dewetting for regime 1 films is presented later. High particle concentration or aggregation may be responsible for arresting further growth of the hole by imparting a solid-like viscoelasticity or contact line pinning or some other mechanism.

**Detailed Structure of Dewetted Droplets.** In order to understand the distribution of the gold nanoparticles within

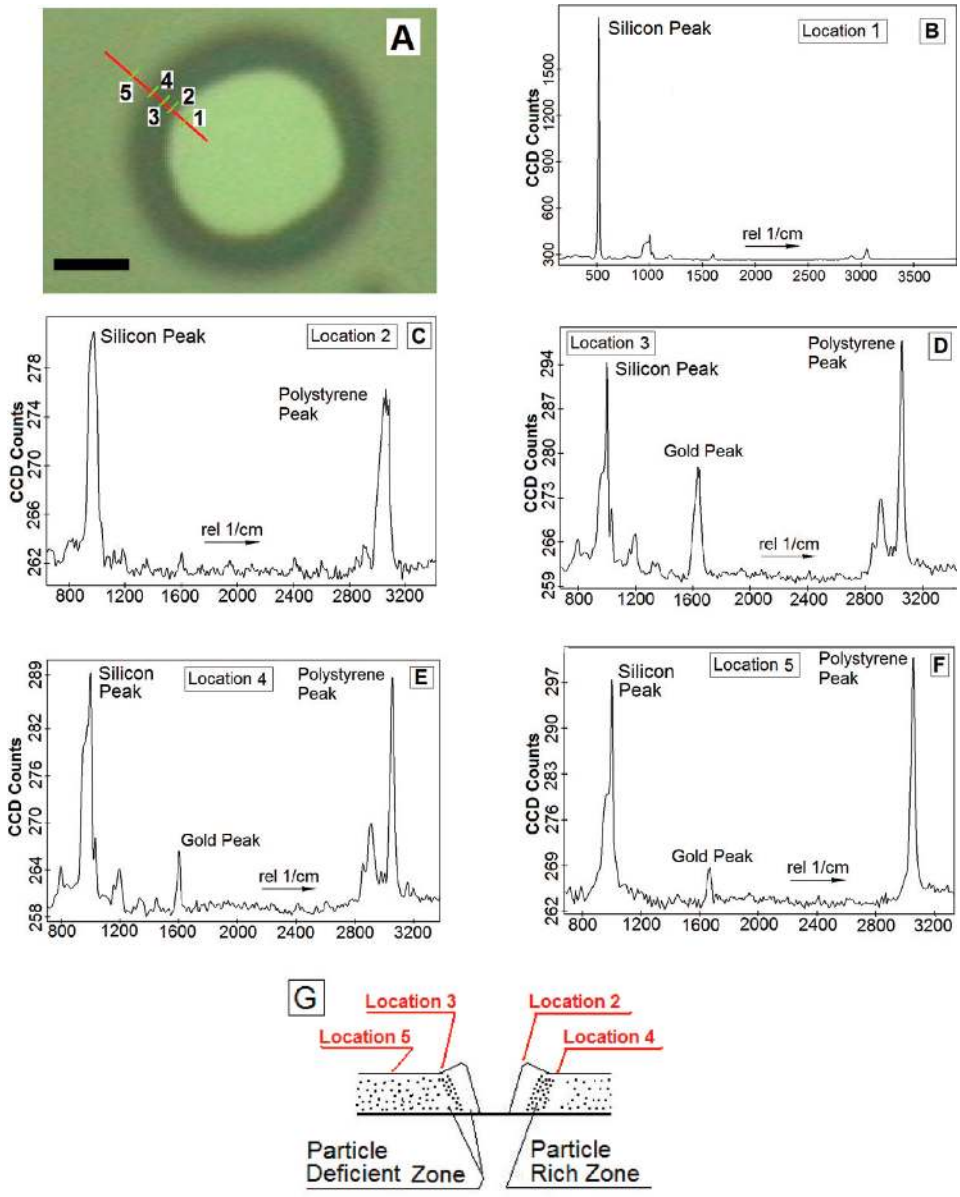


**Figure 5. Detailed micro-Raman analysis of the rim of a regime 2 film. Film thickness is 17 nm, particle concentration is 6.4%. (A) Image of the hole and the locations at which the spectra are taken. (B−F) Spectra at locations 1−5 as marked in (A). (G) Schematic representation of NP distribution around a hole rim.**

each dewetted droplet resulting from the complete dewetting of a regime 1 film, individual droplets were investigated with force modulation AFM (FM-AFM), as well as by micro-Raman analysis. Figure 6 shows the amplitude (A) and the phase (B) contrast image of FM-AFM of a single dewetted droplet revealing its detailed structure. The initial film thickness was 17 nm, and NP concentration was 0.1%. The additional shadow in the FM-AFM image at the center of the droplet calls for special attention. This contrast refers to an aggregate of the gold nanoparticles formed within the dewetted droplet. To further strengthen the indication from the FM-AFM image, micro-Raman imaging of the dewetted droplets was performed, as shown in Figure 7A. Raman spectra from three different locations are taken: location 1 is far from the droplet, over an exposed area of the substrate (Figure 7B); location 2 is close to the periphery of the droplet, away from its

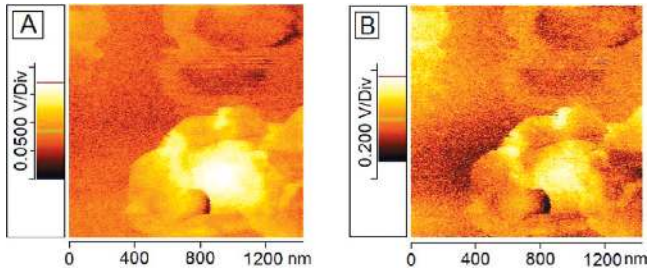


**Figure 6. (A) Amplitude and (B) phase contrast image of force modulation atomic force microscopy image of a single dewetted droplet revealing the detailed core−shell structure. The initial film thickness was 17 nm, and NP concentration was 0.1%.**

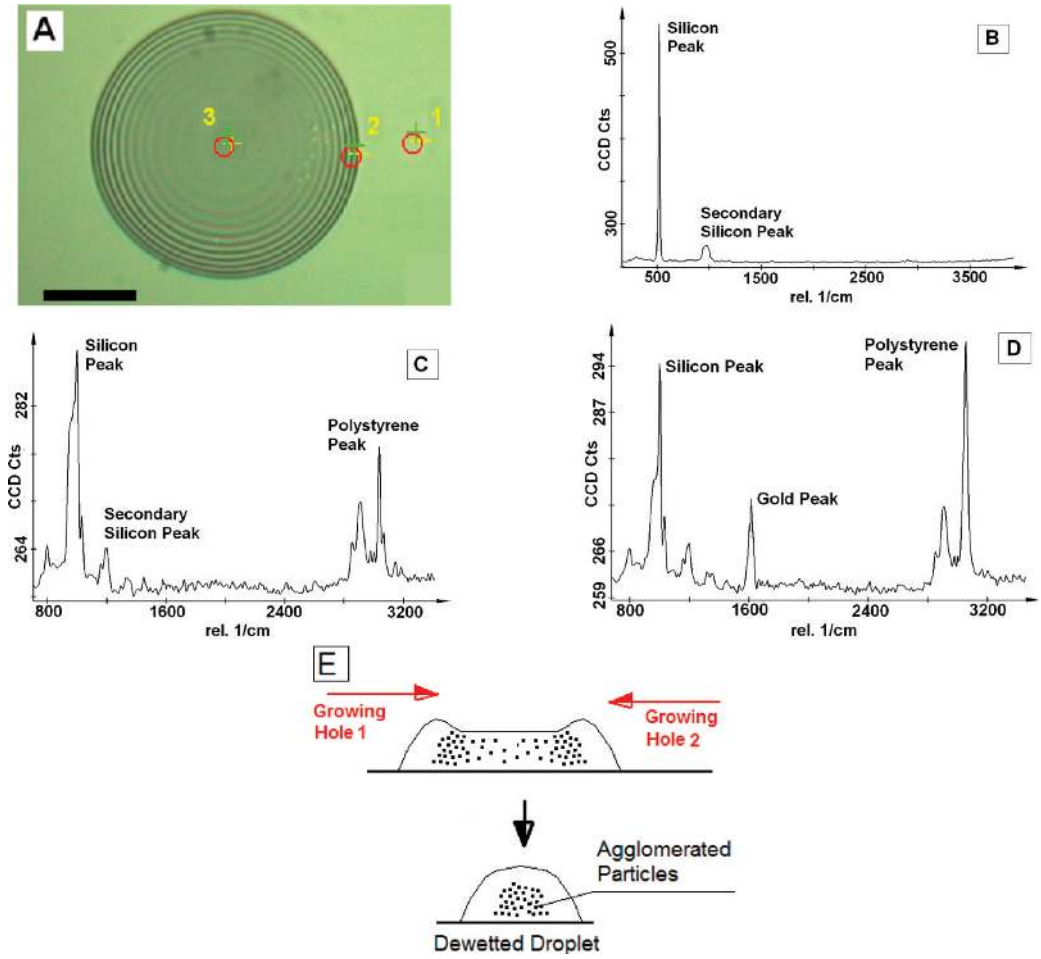


**Figure 7. Micro-Raman analysis results of a single dewetted droplet, resulting from the dewetting of a 17 nm thick regime 1 film with NP concentration of 0.1%. (A) Optical micrograph of the droplet showing the spatial locations where individual spectra have been taken. (B) Spectrum from location 1 (dewetted region), with only the silicon peak. (C) Spectrum from location 2 (edge of the droplet) showing peaks corresponding to silicon (substrate) and polystyrene. (D) Presence of a gold peak in the spectrum from location 3 (center of droplet). (E) Schematic of dynamics of the high NP zone with the retracting contact line during hole growth.**

center (Figure 7C); and location 3 is just above the center of the droplet, the location over which the contrast is seen in the FM-AFM images (Figure 7D). Though only one spectrum corresponding to each location in Figure 7A is shown, spectra were taken from many locations of several fully dewetted droplets to test the repeatability of the results. On the basis of these large numbers of spectra, it could be confirmed that the spectral patterns shown in Figure 7B−D are true representative data for each type of location.

The spectrum in Figure 7B shows only the peak corresponding to silicon. No presence of gold or the polymer (PS) is seen in this particular spectrum. Thus, this spectrum confirms that, for dewetting thin films in regime 1, the gold nanoparticles do not phase separate and accumulate at the film−substrate interface. The spectrum is almost similar to the one shown in Figure 5B, which is from the ruptured portion of the film. The spectra shown in Figures 5B and 7B suggest that there is no phase segregation of the gold particles onto the substrate, as has been observed in some of the systems reported before.[40−50] Both spectra also confirm that dewetting of both regimes 1 and 2 films is clean, as the receding three-phase contact line does not leave behind any remnant polymer or particles on the substrate. The spectrum in Figure 7C corresponds to the edge of a dewetted polymer droplet, which shows the presence of PS, in addition to the peaks corresponding to the silicon wafer substrate buried under the droplet. However, there is no peak here that signifies to the presence of the gold NPs. The spectrum in Figure 7D, which is taken at a location close to the center of the droplet, shows the presence of the gold peak, in addition to the PS and silicon peaks. Thus, on the basis of the FM-AFM image and Raman spectra, we conclude that all of the gold nanoparticles present in each dewetted polymer droplet have aggregated around the center of the droplet. Such aggregation or coarsening of gold nanoparticles in a polymer matrix has been reported very recently, both for homopolymer[77,78] as well as

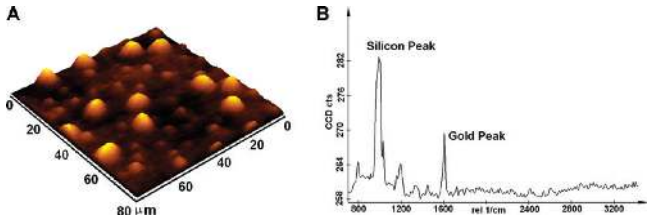


**Figure 8. (A) AFM image of bare aggregates of gold nanoparticles after removal of polystyrene core by selective solvent washing. (B) Micro-Raman spectra over the droplets show the presence of gold and silicon peaks only without the presence of PS.**

for blend nanocomposite films.[79] The process of nanoparticle aggregation and the initial dispersed state are both governed by the Gibbs free energy. Even when aggregation is thermodynamically preferred,[80] kinetics determines if aggregation/segregation can occur over the time scales of instability and dewetting, where a greater negative magnitude of the former makes aggregation more probable. In both cases, the enthalpy part is negative and the entropy part is also negative, making the overall value of Gibbs free energy negative. It appears that the contribution of the entropy term in the expression ($\Delta G = \Delta H - T\Delta S$) has greater contribution to the negative value of Gibbs free energy, making the overall process entropy controlled. In other words, a lower particle−particle cohesive energy penalty, in comparison to a higher energy requirement of particle−polymer adhesion leads to the aggregation of the uncapped nanoparticles, within each dewetted droplet.[80] Interestingly, the aggregation of nanoparticles at the center of the fully dewetted droplets in regime 1 is in accord with the scenario during dewetting of regime 2 films, where it is proposed that gold nanoparticles are somewhat more concentrated in the central part of the rim. However, owing to the lower NP concentrations and less time available for dewetting in regime 1 films, phase segregation is delayed until the merger of the rims to create droplets. As shown schematically in Figure 7E, the rims of two adjacent growing holes coalesce to form a droplet with an NP-rich core in which aggregation can occur over time, resulting in a final dewetted structure having a core−shell-type morphology. The outer shell is of the polymer, and the inner core is made of the aggregated gold nanoparticles. This observation signifies a major difference in the time of particle aggregation between regimes 1 and 2: while aggregation occurs concurrently with dewetting itself in regime 2 films due to longer available time, it takes place after complete dewetting in case of regime 1 films. Such core−shell structure formation may be interesting from the point of patterning as well, as it is not possible to fabricate submerged hierarchical structures by any of the existing top-down lithography techniques.

**Removing the Polymer Shell.** It is evident from the discussion in the previous section that the final dewetted structure in regime 1 films leads to the formation of an isotropic array of core−shell-type structures (Figure 1A, 6A and 7A), comprising a polymer shell and a core made up of aggregated gold nanoparticles. By selective dissolution of the polymer (PS), we could fabricate an array of gold particle aggregates on a flat silicon wafer surface. For this purpose, the dewetted film was carefully washed with cylohexane for prolonged hours (~2−4 h), which resulted in the formation of structures comprising the droplets shown in Figure 8A. Micro-Raman spectra over various areas of the droplets showed the presence of gold and silicon peaks only (Figure 8B). This confirms that the polymer shell has been removed and the resulting structure comprises arrays of self-assembled aggregates of gold nanoparticles. However, it must be admitted that this technique had limited success, as gold particles, during dissolution of the polymer, tend to spread over other areas of the sample, too, as is evident from the presence of a weak gold peak in the spectra taken over the dewetted portions. It may be recalled that there was no presence of such peaks in the spectra taken before washing (Figure 7B). Also, though cylcohexane is not known to be a good solvent for PS,[81] it was deliberately used, as rapid dissolution of PS in stronger solvents such as toluene completely destroyed the gold aggregates. It is the first time that dewetting of a nanocomposite thin film has been utilized to fabricate isolated arrays of gold nanoparticle aggregates. This method is different from the assembly of nanoparticles by dewetting of colloidal solutions containing nanoparticles, aided by macroscopic stick slip motion of the retracting three-phase contact line,[82−84] Further studies on anchoring of dewetted droplets on physicochemically patterned substrates are underway. This may provide a potential method for a precise positioning of core−shell droplets and nanoparticle clusters after removal of the polymer without disturbing the position of the particles.[30]

## CONCLUSIONS

We have critically examined solvent vapor-assisted dewetting of thin (<40 nm) nanocomposite polymer−gold particle films by characterizing the length and time scales of spinodal instability and velocity of hole growth, together with observations of particle concentration. Three distinct stability regimes were detected with different characteristics: (1) films with low nanoparticle concentrations (<~2.0%) dewet completely to form droplets by merger of holes; (2) films with intermediate particle concentrations (3.2−6.4%) show partial dewetting by arrest of an initially growing hole; and (3) films with NP concentrations in excess of 7.0% show complete suppression of instability and dewetting.

The instability length scale and the dimensions of the final dewetted structures in regime 1 are nearly independent of particle concentration, but dynamics of dewetting becomes progressively slower with enhanced nanoparticle concentration. The length scale exponent in this regime is nearly 2, as for pure polymer films without particles. In regime 2, the length scale increases with increase in NP concentration, and its scaling with thickness changes rather drastically to an exponent in the range of 3−3.5. Additionally, the extent to which the dewetting sequence progresses is also found to be dependent on the NP concentrations. For example, while dewetting was found to progress to coalescence of rims with NP concentration of 3.2%, it continued only to the level of formation of a few scattered, isolated holes for films with 6.4% NP concentration. Consistent with all the observations, we propose that arrest of dewetting in regime 2 occurs by aggregation of particles in the central part of a hole rim engendered by higher NP concentration and longer time available for their aggregation in this slow regime. However, the mechanism of transition to regime 2 itself with its anomalous length scale behavior cannot be explained by simple factors such as slippage, viscoelasticity and heterogeneous nucleation. In addition, detailed investigation on dewetting velocity for different NP concentrations in regime 1 films shows that there exist two distinct velocity regimes, particularly for low NP concentrations: a rapid initial phase and a sluggish late stage. Our experiments suggests the presence of slippage in the late stages of dewetting, which is not significant in the earlier phase. As the NP concentration increases, the distinction between the two stages becomes diffused, and for films with 2.0% NP concentration, there was a single regime of velocity over the entire dewetting sequence.

Finally, on the basis of force modulation AFM and micro-Raman analysis, we show that, for the dewetting nanocomposite films in fegime 1, the final dewetted morphology comprises an isotropic array of core−shell-type structure: the shell comprising the dewetted polymer and the core resulting from the self-organized aggregation of the nanoparticles present within a dewetted droplet. Also, the polymer shell could be successfully removed without disturbing the gold aggregates to result in a structure comprising isolated aggregates of gold nanoparticles over a flat silicon wafer substrate.

## METHODS

**Preparation of Gold Nanoparticle Sol.** The synthesis of the gold particles used for this study did not use any kind of capping agent and was achieved only by controlling the rate of the reaction. Tetrahexylammonium bromide (1.74 g) was dissolved in toluene (80 mL) to produce a 50 mM solution. This was combined with a 30 mM solution of hydrogen tetrachloroaurate (0.35 g) in distilled water (30 mL). The suspension was shaken until all the tetrachloroaurate had transferred to the organic phase. A fresh 0.4 M solution of sodium borohydride (0.39 g) in distilled water (25 mL) was prepared and added slowly to the toluene phase. On addition, the color of the toluene phase changed from a clear orange solution to an opaque deep ruby red solution. The lower aqueous phase turned colorless. The mixture was stirred for 30 min before separation and removal of the two phases. The toluene phase was washed with water and dried over $MgSO_4$. Concentration of the solution was 2.54 mg/mL. The preparation method is summarized in a flowchart. The average particle size calculated from TEM analysis was 3.97 ± 0.45 nm (image not shown, details can be found elsewhere).[85]

**Preparation of Gold Nanoparticle Filled Polystyrene Films.** Toluene is one of the common solvents for polystyrene, and so, bids of monodispersed PS (Sigma Aldrich, UK, molecular weight = 280K, polydispersity index (PDI) <1.1) were directly added to the gold sol stabilized in toluene for making PS solution containing gold nanoparticles. The concentration of the particles was calculated as the ratio of the weights of gold nanoparticles present in the system to that of the polymer added. The PS solution in the toluene sol was directly spin coated on clean single-sided polished n-type commercial grade silicon wafer (Wafer World Inc., USA) pieces. For this study, films having thicknesses of 12 ± 0.3, 15 ± 0.3, 17 ± 0.6, 20 ± 0.4, 23 ± 0.4, 26 ± 0.6, 30 ± 0.2, 34 ± 0.8, and 42 ± 0.9 nm with nanoparticle concentrations of 0.04, 0.1, 1.0, 2.0, 3.2, 4.0, 5.0, 6.4, 7.0, and 8.0% as well as 0% (PS films without any nanoparticle) for each thickness are used. The film thicknesses were controlled by varying the concentrations of the PS solution, the spin speed, and the duration of spinning to a lesser extent. The film thicknesses were measured using an imaging ellipsometer (EP3, Nanofilm Germany).

One major concern with the coated films was to ensure that the particles did not phase segregate during the film preparation stage. This was verified by TEM imaging of the coated films, which clearly showed that the particles had not phase segregate in the films. The details of the methodology adopted for this particular characterization is available in Supporting Information.

**Dewetting Experiments.** The dewetting of the films was engendered by exposure to toluene vapor in a closed glass chamber presaturated with toluene vapor. Exposing a polymer film to its solvent vapor effectively reduces the glass transition temperature due to penetration of the solvent molecules into the film matrix. The absorption of solvent into the polymer matrix leads to increase in its free volume, resulting in reduced cohesion between the polymer molecules, which in turn aids their mobility.[29] Thus, the molecules become free to reorganize and depending on the thermodynamics of the system can lead to the rupture and dewetting of the thin film. Minimization of the excess free energy is the key motivation for the self-organization. The evolution sequence of the films were observed under an optical microscope (Leica DMLM) in reflection mode, and images were captured with a CCD camera (Samsung) mounted to the microscope.

The aggregation of gold nanoparticles within dewetted droplets was analyzed by the WiTec CRM 200 Raman spectrometer coupled with a high-resolution confocal optical microscope. With this combination, it is possible not only to obtain a Raman spectrum of a sample but also to combine its chemical constitution with a lateral resolution in the submicrometer regime. Both the excitation and collection of the scattered light were done through the microscope objective. Excitation was provided by the 514.5 nm line of an $Ar^+$ laser. The microscope objective used was Nikon 100×, with a working distance of 0.26. Thus, the laser beam diameter and power at the focus were ~500 nm and 2 mW, respectively. All measurements were made at room temperature, in order to avoid heating effects in the spectra. Therefore, the measurements were performed at a laser power density below threshold to induce temperature enhancement. All of the measured spectra were systematically compared to those obtained on a coverslip under the same experimental conditions.

Force modulation (FM) imaging is a secondary imaging technique based on contact mode atomic force microscopy that identifies and maps differences in surface stiffness or elasticity. These techniques probe various surface properties to differentiate between the different materials that make up heterogeneous surfaces. In force modulation, the probe moves with a small vertical (*z*) oscillation (modulation), which is significantly faster than the raster scan rate. The force on the sample is modulated such that the average force on the sample is equal to that in contact mode. When the probe is modulated with the tip in contact with a sample, the sample surface resists the oscillation and the cantilever bends. Under the same force, a stiff area on the sample deforms less than a soft area; that is, stiffer areas put up greater resistance to the cantilever's vertical oscillation and, consequently, cause greater bending of the cantilever. The variation in cantilever deflection amplitude at the frequency of modulation is a measure of the relative stiffness of the surface. Topographical information (DC, or non-oscillatory deflection) is collected simultaneously with the force modulation data (AC, or oscillatory deflection). Here, this technique has been used to show the presence of both gold NP aggregates and PS in the dewetted droplet. For FM-AFM, we have used a Si cantilever with a spring constant (*k*) of 3 N/m. The resonance frequency of the cantilever was ~75 kHz (according to the manufacturer's datasheet).

In order to ascertain the repeatability of the results, at least three samples of each thickness and particle concentrations were used in the experiments. The number density of the holes is counted at three to five locations for each sample, and thus, the mean and the error bars reported in the texts or shown in the plots are based on averaging over 10 to 15 values obtained for a single thickness−particle concentration combination.

*Acknowledgment.* A.S., A.K.R., R.M., and S.D. acknowledge the support of the Department of Science & Technology (DST), New Delhi, a DST IRPHA grant (A.S.), and a DST Fast track project (R.M.).

*Supporting Information Available:* Additional experimental details and figures. This material is available free of charge *via* the Internet at http://pubs.acs.org.

## REFERENCES AND NOTES


1. Singh, J.; Agrawal, K. K. Polymeric Materials for Contact Lenses. *J. Macromol. Sci.* **1992**, *32*, 521–534.
2. Mayer, W. H. Polymer Electrolytes for Lithium-Ion Batteries. *Adv. Mater.* **1998**, *10*, 439–448.
3. Friend, R. H.; Gymer, R. W.; Holmes, A. B.; Burroughs, J. H.; Marks, R. N.; Taliani, C.; Bradley, D. D. C.; Dos Santos, D. A.; Breads, J. L.; Logdlund, M. L.; Salaneck, W. R. Electroluminescence in Conjugated Polymers. *Nature* **1999**, *397*, 121–128.
4. Kelley, T. W.; Baude, P. F.; Gerlach, C.; Ender, D. E.; Muyres, D.; Haase, M. A.; Vogel, D. E.; Theiss, S. D. Recent Progress in Organic Electronics: Materials, Devices, and Processes. *Chem. Mater.* **2004**, *16*, 4413–4422.
5. Reiter, G. Dewetting of Thin Polymer Films. *Phys. Rev. Lett.* **1992**, *68*, 75–78.
6. Reiter, G. Unstable Thin Polymer Films: Rupture and Dewetting Processes. *Langmuir* **1993**, *9*, 1344–1351.
7. Redon, C.; Brochard-Wyart, F.; Rondelez, F. Dynamics of Dewetting. *Phys. Rev. Lett.* **1991**, *66*, 715–718.
8. Morariu, M. D.; Schaffer, E.; Steiner, U. Molecular Forces Caused by the Confinement of Thermal Noise. *Phys. Rev. Lett.* **2004**, *92*, 156102.
9. Sharma, A.; Ruckenstein, E. Mechanism of Tear Film Rupture and Formation of Dry Spots on Cornea. *J. Colloid Interface Sci.* **1985**, *106*, 12–27.
10. Sharma, A.; Reiter, G. Instability of Thin Polymer Films on Coated Substrates: Rupture, Dewetting and Drop Formation. *J. Colloid Interface Sci.* **1996**, *178*, 383–399.
11. Sharma, A.; Khanna, R. Pattern Formation in Unstable Thin Liquid Films. *Phys. Rev. Lett.* **1998**, *81*, 3463–3466.
12. Sharma, A. Many Paths to Dewetting of Thin Films: Anatomy and Physiology of Surface Instability. *Eur. Phys. J. E* **2003**, *12*, 397–408.
13. Seeman, R.; Herminghaus, S.; Jacobs, K. Dewetting Patterns and Molecular Forces: A Reconciliation. *Phys. Rev. Lett.* **2001**, *86*, 5534–5537.
14. Becker, J.; Grun, G.; Seemann, R.; Mantz, H.; Jacobs, K.; Mecke, K. R.; Blossey, R. Complex Dewetting Scenarios Captured by Thin-Film Models. *Nat. Mater.* **2002**, *2*, 59–63.
15. Seemann, R.; Herminghaus, S.; Neto, C.; Schlagowski, S.; Podzimek, D.; Konrad, R.; Mantz, H.; Jacobs, K. Dynamics and Structure Formation in Thin Polymer Melt Films. *J. Phys.: Condens. Matter* **2005**, *17*, S267–S290.
16. Oron, M.; Kerle, T; Yarushalmi-Rozen, R.; Klein, J. Persistent Droplet Motion in Liquid−Liquid Dewetting. *Phys. Rev. Lett.* **2004**, *92*, 236104.
17. Konnur, R.; Kargupta, K.; Sharma, A. Instability and Morphology of Thin Liquid Films on Chemically Heterogeneous Substrates. *Phys. Rev. Lett.* **2000**, *84*, 931–934.
18. Tsui, O. K. C.; Wang, Y. J.; Zhao, H.; Du, B. Some Views about the Controversial Dewetting Morphology of Polystyrene. Films. *Eur. Phys. J. E* **2003**, *12*, 417–425.
19. Karapanageotis, I.; Gerberich, W. W. A Criterion for Dewetting Initiation from Surface Disturbances on Ultrathin Polymer Films. *Langmuir* **2005**, *21*, 9194–9198.
20. Reiter, G.; Hamieh, M.; Damman, P.; Sclavons, S. E.; Gabriele, S.; Vilmin, T.; Raphael, E. Residual Stresses in Thin Polymer Films Cause Rupture and Dominate Early Stages of Dewetting. *Nat. Mater.* **2005**, *4*, 754–758.
21. Damman, P.; Gabriele, S.; Coppee, S.; Desprez, S.; Villers, D.; Vilmin, T.; Raphae, E.; Hamieh, M.; Al Akhrass, S.; Reiter, G. Relaxation of Residual Stress and Re-entanglement of Polymers in Spin-Coated Films. *Phys. Rev. Lett.* **2007**, *99*, 036101.
22. Sharma, A.; Mittal, J. Instability of Thin Liquid Films by Density Variations: A New Mechanism that Mimics Spinodal Dewetting. *Phys. Rev. Lett.* **2002**, *89*, 186101.
23. Sharma, A.; Mittal, J.; Verma, R. Instability and Dewetting of Thin Films Induced by Density Variations. *Langmuir* **2002**, *18*, 10213–10220.
24. Kargupta, K.; Sharma, A. Templating of Thin Films Induced by Dewetting on Patterned Surfaces. *Phys. Rev. Lett.* **2001**, *86*, 4536–4539.
25. Kargupta, K.; Sharma, A. Morphological Self-Organization by Dewetting in Thin Films on Chemically Patterned Substrates. *J. Chem. Phys.* **2002**, *116*, 3042–3051.
26. Kargupta, K.; Sharma, A. Mesopatterning of Thin Liquid Films by Templating on Chemically Patterned Complex Substrates. *Langmuir* **2003**, *19*, 5153–5163.
27. Mayer, E.; Braun, H.-G. Controlled Dewetting Pprocesses on Microstructured Surfaces—A New Procedure for Thin Film Microstructuring. *Macromol. Mater. Eng.* **2000**, *276/277*, 44–50.
28. Sehgal, A.; Ferreiro, V.; Douglas, J. F.; Amis, E. J.; Karim, A. Pattern-Directed Dewetting of Ultrathin Polymer Films. *Langmuir* **2002**, *18*, 7041–7048.
29. Mukherjee, R.; Gonuguntla, M.; Sharma, A. Meso-Patterning of Thin Polymer Films by Controlled Dewetting: From Nano-Droplet Arrays to Membranes. *J. Nanosci. Nanotechnol.* **2007**, *7*, 2069–2075.
30. Mukherjee, R.; Bandopadhyay, D.; Sharma, A. Control of Morphology in Pattern Directed Dewetting of Thin Polymer Films. *Soft Matter* **2008**, *4*, 2086–2097.
31. Wang, J. Z.; Zheng, Z. H.; Li, H. W.; Huck, W. T. S.; Sirringshaus, H. Polymer Field Effect Transistors Fabricated by Dewetting. *Synth. Met.* **2004**, *146*, 287–290.
32. Benor, A.; Hoppe, A.; Wagner, V.; Knipp, D. Microcontact Printing and Selective Surface Dewetting for Large Area Electronic Applications. *Thin Solid Films* **2007**, *515*, 7679–7682.
33. Carnazza, S.; Satriano, S.; Guglielmino, S. Self-Organization of Yeast Cells on Modified Polymer Surfaces after Dewetting: New Perspectives in Cellular Patterning. *J. Phys.: Condens. Matter* **2006**, *18*, S2221–S2230.

34. Yerushalmi-Rozen, R.; Klein, J.; Fetters, L. J. Suppression of Rupture in Thin, Nonwetting Liquid Films. *Science* **1994**, *263*, 793–795.
35. Henn, G.; Bucknall, D. G.; Stamm, M.; Vanhoorne, P.; Jerome, R. Chain End Effects and Dewetting in Thin Polymer Films. *Macromolecules* **1996**, *29*, 4305–4313.
36. Feng, Y.; Karim, A.; Weiss, R. A.; Douglas, J. F.; Han, C. C. Control of Polystyrene Film Dewetting through Sulfonation and Metal Complexation. *Macromolecules* **1998**, *31*, 484–493.
37. Li, X.; Han, Y.; An, L. Inhibition of Thin Polystyrene Film Dewetting *via* Phase Separation. *Polymer* **2003**, *44*, 5833–5841.
38. Kropka, J. M.; Green, P. F. Control of Interfacial Instabilities in Thin Polymer Films with the Addition of a Miscible Component. *Macromolecules* **2006**, *39*, 8758–8762.
39. Carroll, G. T.; Sojka, M. E.; Lei, X.; Turro, N. J.; Koberstein, J. T. Photoactive Additives for Cross-Linking Polymer Films: Inhibition of Dewetting in Thin Polymer Films. *Langmuir* **2006**, *22*, 7748–7754.
40. Barnes, K. A.; Karim, A.; Douglas, J. F.; Nakatani, A. I.; Gruell, H.; Amis, E. J. Suppression of Dewetting in Nanoparticle-Filled Polymer Films. *Macromolecules* **2000**, *33*, 4177–4185.
41. Krishnan, R. S.; Mackay, M. E.; Hawker, C. J.; Van Horn, B. Influence of Molecular Architecture on the Dewetting of Thin Polystyrene Films. *Langmuir* **2005**, *21*, 5770–5776.
42. Mackay, M. E.; Hong, Y.; Jeong, M.; Hong, S.; Russell, T. P.; Hawker, C. J.; Vestberg, R.; Douglas, J. F. Influence of Dendrimer Additives on the Dewetting of Thin Polystyrene Films. *Langmuir* **2002**, *18*, 1877–1882.
43. Luo, H.; Gersappe, D. Dewetting Dynamics of Nanofilled Polymer Thin Films. *Macromolecules* **2004**, *37*, 5792–5799.
44. Hosaka, N.; Tanaka, K.; Otsuka, H.; Otsuka, H.; Takahara, A. Influence of the Addition of Silsesquioxane on the Dewetting Behavior of Polystyrene Thin Film. *Compos. Interfaces* **2004**, *11*, 297–306.
45. Kropka, J. M.; Garcia Sakai, V.; Green, P. F. Local Polymer Dynamics in Polymer−$C_{60}$ Mixtures. *Nano Lett.* **2008**, *8*, 1061–1065.
46. Sharma, S.; Rafailovich, M. H.; Peiffer, D.; Sokolov, J. Control of Dewetting Dynamics by Adding Nanoparticle Fillers. *Nano Lett.* **2001**, *1*, 511–514.
47. Xavier, J. H.; Sharma, S.; Seo, Y. S.; Isseroff, R.; Koga, T.; White, H.; Ulman, A.; Shin, K.; Satija, S. K.; Sokolov, J.; Rafailovich, M. H. Effect of Nanoscopic Fillers on Dewetting Dynamics. *Macromolecules* **2006**, *39*, 2972–2980.
48. Koo, J; Shin, K.; Seo, Y.-S.; Koga, T.; Park, S.; Satija, S.; Chen, X.; Yoon, K.; Hsiao, B. S.; Sokolov, J. C.; Rafailovich, M. H. Stabilizing Thin Film Polymer Bilayers against Dewetting Using Multiwalled Carbon Nanotubes. *Macromolecules* **2007**, *40*, 9510–9516.
49. Cole, D. H.; Shull, K. R.; Baldo, P.; Rehn, L. Dynamic Properties of a Model Polymer/ Metal Nanocomposite: Gold Particles in Poly(*tert*-butyl acrylate). *Macromolecules* **1999**, *32*, 771–779.
50. Hosaka, N.; Tanaka, K.; Otsuka, H.; Otsuka, H.; Takahara, A. Structure and Dewetting Behavior of Polyhedral Oligomeric Silsesquioxane-Filled Polystyrene Thin Films. *Langmuir* **2007**, *23*, 902–907.
51. Oh, H.; Green, P. F. Polymer Chain Dynamics and Glass Transition in a Thermal Polymer/Nanoparticle Mixtures. *Nat. Mater.* **2008**, *8*, 139–143.
52. Kropka, J. M.; Putz, K. W.; Pryamitsyn, V.; Ganesan, V.; Green, P. F. Origin of Dynamical Properties in PMMA−$C_{60}$ Nanocomposites. *Macromolecules* **2007**, *40*, 5424–5432.
53. Krishnamoorti, R.; Vaia, R. A.; Giannelis, E. P. Structure and Dynamics of Polymer-Layered Silicate Nanocomposites. *Chem. Mater.* **1996**, *8*, 1728–1734.
54. Krishnamoorti, R.; Giannelis, E. P. Rheology of End-Tethered Polymer Layered Silicate Nanocomposites. *Macromolecules* **1997**, *30*, 4097–4102.
55. Yurekli, K.; Krishnamoorti, R.; Tse, M. F.; McElrath, K. O.; Tsou, A. H.; Wang, H. C. Structure and Dynamics of Carbon Black-Filled Elastomers. *J. Polym. Sci. B: Polym. Phys.* **2000**, *39*, 256–275.
56. Mackay, M. E.; Dao, T. T.; Tuteja, A.; Ho, D. L.; Van Horn, B.; Kim, H.-C.; Hawker, C. J. Nanoscale Effects Leading to Non-Einstein-like Decrease in Viscosity. *Nat. Mater.* **2003**, *2*, 762–766.
57. Watanabe, H.; Inoue, T. Role of Chain Connectivity in Viscoelastic Properties of Polymeric Liquids: A Review. *Mater. Sci. Eng. A* **2006**, *442*, 361–366.
58. Tuteja, A.; Mackay, M. E.; Hawker, C. J.; Van Horn, B. Effect of Ideal, Organic Nanoparticles on the Flow Properties of Linear Polymers: Non-Einstein-like Behavior. *Macromolecules* **2005**, *38*, 8000–8011.
59. Du, F.; Scogna, R. C.; Zhou, W.; Brand, S.; Fischer, J. E.; Winey, K. I. Nanotube Networks in Polymer Nanocomposites: Rheology and Electrical Conductivity. *Macromolecules* **2004**, *37*, 9048–9055.
60. Zhang, Q.; Archer, L. A. Poly(ethylene oxide)/Silica Nanocomposites: Structure and Rheology. *Langmuir* **2002**, *18*, 10435–10442.
61. Lozano, K.; Bonilla-Rios, J.; Barrera, E. V. A Study on Nanofiber-Reinforced Thermoplastic Composites (II): Investigation of the Mixing Rheology and Conduction Properties. *J. Appl. Polym. Sci.* **2000**, *80*, 1162–1172.
62. Potschke, P.; Fornes, T. D.; Paul, D. R. Rheological Behavior of Multiwalled Carbon Nanotube/Polycarbonate Composites. *Polymer* **2002**, *43*, 3247–3255.
63. Schaffer, E.; Thurn-Albrecht, T.; Russell, T. P.; Steiner, U. Electrically Induced Structure Formation and Pattern Transfer. *Nature* **2000**, *403*, 874–877.
64. Harkema, S.; Schaffer, E.; Morariu, M. D.; Steiner, U. Pattern Replication by Confined Dewetting. *Langmuir* **2003**, *19*, 9714–9718.
65. Israelachvili, J. *Intermolecular Surface Forces*, 2nd ed.; Academic Press: New York, 1992.
66. Sarkar, J.; Sharma, A. A Unified Theory of Instabilities in Viscoelastic Thin Films: From Wetting to Confined Films, From Viscous to Elastic Films, and From Short to Long Waves. *Langmuir* **2010**, *26*, 8464−8473.
67. Arun, N.; Sharma, A.; Pattader, P. S. G.; Banerjee, I.; Dixit, H. M.; Narayan, K. S. Electric Field Induced Patterns in Soft Visco-Elastic Films: From Long Waves of Viscous Liquids to Short Waves of Elastic Solids. *Phys. Rev. Lett.* **2009**, *102*, 254502.
68. Tomar, G.; Shankar, V.; Sharma, A.; Biswas, G. Electrohydrodynamic Instability of a Confined Viscoelastic Liquid Film. *J. Non-Newtonian Fluid Mech.* **2007**, *143*, 120–130.
69. Kargupta, K.; Sharma, A.; Khanna, R. Instability, Morphology and Dynamics of Thin Slipping Films. *Langmuir* **2004**, *20*, 244–253.
70. Sharma, A.; Kargupta, K. Instability and Dynamics of Thin Slipping Films. *Appl. Phys. Lett.* **2003**, *83*, 3549–3551.
71. Shenoy, V.; Sharma, A. Stability of a Thin Elastic Film Interacting with a Contactor. *J. Mech. Phys. Solids* **2002**, *50*, 1155–1173.
72. Tomar, G.; Shankar, V.; Shukla, A.; Sharma, A.; Biswas, G. Instability and Dynamics of Thin Viscoelastic Liquid Films. *Euro. Phys. J. E* **2006**, *20*, 185–200.
73. Brochard-Wyart, F.; Debrégeas, G.; Fondecave, R.; Martin, P. Dewetting of Supported Viscoelastic Polymer Films: Birth of Rims. *Macromolecules* **1997**, *30*, 1211–1213.
74. Masson, J.-L.; Green, P. F. Hole Formation in Thin Polymer Films: A Two-Stage Process. *Phys. Rev. Lett.* **2002**, *88*, 205504.
75. Jacobs, K.; Seemann, R.; Schatz, G.; Herminghaus, S. Growth of Holes in Liquid Films with Partial Slippage. *Langmuir* **1998**, *14*, 4961–4963.
76. Al Akhrass, S.; Reiter, G.; Hou, S. Y.; Yang, M. H.; Chang, Y. L.; Chang, F. C.; Wang, C. F.; Yang, A. C.-M. Viscoelastic Thin Polymer Films under Transient Residual Stresses: Two-Stage Dewetting on Soft Substrates. *Phys. Rev. Lett.* **2008**, *100*, 178301.
77. Meli, L.; Green, P. F. Aggregation and Coarsening of Ligand-Stabilized Gold Nanoparticles in Poly(methyl methacrylate) Thin Films. *ACS Nano* **2008**, *2*, 1305–1312.
78. Han, J. T.; Lee, G. W.; Kim, S.; Lee, H. J.; Douglas, J. F.; Karim,

A. Direct Observation of Interfacial $C_{60}$ Cluster Formation in Polystyrene−$C_{60}$ Nanocomposite Films. *Nanotechnology* **2009**, *20*, 105705.
79. Chung, H. J.; Ohno, K.; Fukuda, T.; Composto, R. J. Internal Phase Separation Drives Dewetting in Polymer Blend and Nanocomposite Films. *Macromolecules* **2007**, *40*, 384–388.
80. McGarrity, E. S.; Duxbury, P. M.; Mackay, M. E.; Frischknecht, A. L. Calculation of Entropic Terms Governing Nanoparticle Self-Assembly in Polymer Films. *Macromolecules* **2008**, *41*, 5952–5954.
81. Harton, S. E.; Luning, J.; Betz, H.; Ade, H. Polystyrene/Poly(methyl methacrylate) Blends in the Presence of Cyclohexane: Selective Solvent Washing or Equilibrium Adsorption. *Macromolecules* **2006**, *39*, 7729–7733.
82. Lee, L.-T.; Leite, C. A. P.; Galembeck, F. Controlled Nanoparticle Assembly by Dewetting of Charged Polymer Solutions. *Langmuir* **2004**, *20*, 4430–4435.
83. Lu, N.; Chen, X.; Molenda, D.; Naber, A.; Fuchs, H.; Talapin, D. V.; Weller, H.; Mller, J.; Lupton, J. M.; Feldmann, J.; Rogach, A. L.; Chi, L. Lateral Patterning of Luminescent CdSe Nanocrystals by Selective Dewetting from Self-Assembled Organic Templates. *Nano Lett.* **2004**, *4*, 885–888.
84. Huang, J.; Kim, F.; Tao, A. R.; Connor, S.; Yang, P. Spontaneous Formation of Nanoparticle Stripe Patterns through Dewetting. *Nat. Mater.* **2005**, *4*, 896–900.
85. Das, A.; Das, S.; Raychaudhuri, A. K. Growth of Two-Dimensional Arrays of Uncapped Gold Nanoparticles on Silicon Substrates. *Bull. Mater Sci.* **2008**, *31*, 277–282.